Published in "The Journal of Chemical Physics 139(13): 134302, 2014"
which should be cited to refer to this work.

Dissociation of chloromethanes upon resonant σ^* excitation studied by x-ray scattering

R. Bohinc,[1,a)] M. Žitnik,[1,2] K. Bučar,[1] M. Kavčič,[1] L. Journel,[3] R. Guillemin,[3] T. Marchenko,[3] M. Simon,[3] and W. Cao[4,5,6]
[1]*Jožef Stefan Institute, Jamova cesta 39, SI-1000 Ljubljana, Slovenia*
[2]*Faculty of Mathematics and Physics, University of Ljubljana, Jadranska ulica 19, SI-1000 Ljubljana, Slovenia*
[3]*UPMC, Université Paris 06, CNRS, UMR 7614, LCPMR, 11 rue Pierre et Marie Curie, 75231, Paris Cedex 05, France*
[4]*Department of Physics, University of Oulu, P.O. Box 3000, FIN-90014 Oulu, Finland*
[5]*Department of Physics, University of Fribourg, Ch-1700 Fribourg, Switzerland*
[6]*Department of Chemistry, 110 Science Place, Saskatoon, Saskatchewan S7N 5C9, Canada*

The dissociation process following the Cl K-shell excitation to σ^* resonances is studied by high resolution spectroscopy of resonant elastic and inelastic x-ray scattering on CH_3Cl, CH_2Cl_2, $CHCl_3$, and CCl_4 molecules. Calculations employing the transition potential and Delta-Kohn-Sham DFT approach are in good agreement with the measured total fluorescence yield and show the presence of a second quasidegenerate group of states with σ^* character above the lowest σ^* unoccupied molecular orbital for molecules with more than one Cl atom. A bandwidth narrowing and a nonlinear dispersion behavior is extracted from the Kα spectral maps for both σ^* resonances. The fitted data indicate that the widths of the Franck-Condon distributions for the first and second σ^* resonances are comparable for all the molecules under study. In addition, an asymmetric broadening of the emission peaks is observed for resonant elastic x-ray scattering with zero detuning on both σ^* resonances. This is attributed to the fast dissociation, transferring about 0.15 of the scattering probability into higher vibrational modes.

I. INTRODUCTION

Chlorinated methane derivatives form the simplest group of chlorinated hydrocarbons (CHCs) that are present in natural systems, as well as in the chemical industry. Because of the high reactivity of the C–Cl bond they are excellent synthesis intermediates and can be thought of as basic building blocks of modern polymers, for example, PVC ($CHCl{=}CH_2$), PVDC ($CCl_2{=}CH_2$), PVDF ($CCl_3{-}CH_3$), ….[1] Due to their high volatility CHCs are interesting solvents, and despite their reduced consumption, they remain essential for certain applications.

Due to their unambiguous importance, chloromethanes have been studied by a number of x-ray techniques. In a systematic study employing photoelectron spectroscopy, potential barrier effects, and extended x-ray absorption fine structure (EXAFS) oscillations were studied in the vicinity of carbon K and chlorine $L_{2,3}$ and L_1 edges.[2] In the case of carbon 1*s* excitations, a strong influence of the number of chlorine atoms in the molecule on the suppression of Rydberg and enhancement of valence resonances was found, much like in SF_6.[3] In another work noticeable shifts in the 2*s* and 2*p* ionization potentials and Auger KLL emission spectra were found to be related to the electronegativity of chloromethanes.[4,5] On the other hand, only subtle effects of the chemical environment on Kα and Kβ spectra were reported in above K edge emission studies,[6,7] indicating a similarity in the electronic structure of occupied valence orbitals. Since CHCs are chemically related to freons, responsible for the depletion of the ozone layer observed in the early 1980s,[8,9] a lot of x-ray studies were focused at the differences between small molecules with different number of chlorine, fluorine, and hydrogen atoms in the recent years.[10–14] While the chlorine 1*s* spectra seemed to be only mildly affected by the interchange of chlorine, fluorine, and hydrogen atoms due to the strong localization of the core-hole, a strong influence of the ligand choice on the carbon 1*s* and chlorine 2*p* spectra was found. This influence has recently also been studied in the carbon 1*s* photoelectron spectra of chlorinated ethanes.[15,16] A nonstoichiometric ratio of intensities of photoelectron peaks coming from two nonequivalent carbon atoms in the molecule, which exhibits EXAFS-like oscillations, as well as the electron angular distribution have been shown to depend on the chemical environment of the carbon atom.

It has been known for a while that the promotion of a core electron to a strongly antibonding σ^* type orbital can result in the fast dissociation of the molecule.[17–19] While Auger spectroscopy is the preferred tool for studying photo-induced dissociation in the soft x-ray region,[20,21] resonant elastic, and inelastic x-ray scattering (REXS, RIXS) can successfully be applied in the x-ray energy above a few keV region, where a significant part of core-holes decays radiatively. The first RIXS and REXS observation of dissociation following photoexcitation in the tender x-ray region has been performed by Simon *et al.*,[22] where femtosecond nuclear

a)Author to whom correspondence should be addressed. Electronic mail: rok.bohinc@ijs.si

dynamics was observed after excitation along the Cl $1s \rightarrow \sigma^*$ resonance in gas phase HCl. The interplay between dissociation and emission resulting in an observable breakdown of linear Raman-like dispersion and narrowing of emission lines in RIXS spectra, and an asymmetrical peak broadening in REXS spectra has previously been explained.[23,24] Since then, several RIXS studies on dissociative states involving interference effects,[25] RIXS based electronegativity scale,[26] and molecular field effects[11,27] have been performed.

All of these studies were carried out on an intense first resonance involving core excitations to the lowest unoccupied molecular orbital (LUMO) of antibonding σ^*-type character. For example, in the case of CH_3Cl the LUMO orbital mainly consists of the chlorine $3p$ and carbon $2p/2s$ orbitals both directed along the C–Cl bond. If however more than one halogen atom is present in the molecule, another quasidegenerate group of σ^*-type orbitals is formed. These orbitals are denoted here as 2nd σ^* orbitals/resonances and promotion of a core electron to those unoccupied orbitals is expected to result in fast dissociation of the molecule. A experimental confirmation of this hypothesis can be found by looking at the carbon $1s$ photoelectron spectra of CCl_4.[2] Since excitation to the LUMO is dipole forbidden in the tetrahedral symmetry, the first resonance in the spectrum is mainly attributed to excitations to LUMO+1 of σ^* character. This resonance is much broader than other Rydberg-type resonances indicating the existence of another process through which energy can be dispersed. In other less symmetric molecules the 1st and 2nd σ^* resonances partially overlap and because the 1st σ^* resonance is much more intense than the 2nd σ^* resonance, it is hard to determine its width from x-ray absorption or photoelectron spectra. On the other hand, RIXS spectral maps carry enough information to quantitatively extract the characteristic resonance parameters. Recently, the width of the Franck-Condon distribution (FC width) for the σ^* resonance in CH_3I was determined from the RIXS measurements following the excitation of the iodine L_2 and L_3 core electrons into this very short-lived core-excited state (200 as Ref. 28).

In this paper, we report a study on the dissociation dynamics of CH_3Cl, CH_2Cl_2, $CHCl_3$, and CCl_4 after promotion of Cl $1s$ electron to the 1st and 2nd σ^* orbitals. The paper is structured as follows. The experimental setup and the data acquisition are described in Sec. II. Section III is introduced by the description of the electronic ground-state configuration for chloromethanes, followed by the description of the computational method used to model the experimental absorption spectra. In Sec. IV, the present total fluorescence yield (TFY), RIXS, and REXS results are discussed in detail, and the final conclusions are gathered in Sec. V. The corrections of the emission spectra due to the target self-absorption, the estimation of the experimental resolution and the expressions for the absorption and emission cross sections are presented in Appendixes A, B, and C, respectively.

II. EXPERIMENTAL DETAILS

All the TFY, RIXS, and REXS measurements on chloromethanes in the gas phase at room temperature were performed at the ID26 beamline of the European Synchrotron Radiation Facility (ESRF). RIXS measurements on CH_3Cl were performed separately in a different experiment[28] preceding the measurements on CH_2Cl_2, $CHCl_3$, and CCl_4. The experimental setup was however the same for all molecules (Figure 1) and was described in detail previously.[29] Essentially, a linearly polarized beam with a flux of $\sim 5 \times 10^{12}$ photons/s, $250 \times 50\ \mu m^2$ cross section and full width at half maximum (FWHM) energy width of $\delta_P = 0.4$ eV[28] passed through a stainless steel gas cell separated from vacuum by 12.5 μm thick kapton windows and filled with the sample at the vapor pressure of approximately 30 mbar. Scattered photons were collected in the horizontal plane at 90° with respect to the direction of incoming light along its horizontal polarization direction employing a photodiode to measure the TFY and a crystal spectrometer to analyze the energies of the scattered photons. To measure RIXS K_α and REXS spectra, the first order reflection from a Si(111) crystal bent in Johansson geometry with a 500 mm Rowland circle radius was used together with a position sensitive detection of photons by a thermoelectrically cooled CCD camera (−40 °C, $22.5 \times 22.5\ \mu m^2$ pixel size). For each molecule the measured RIXS (REXS) spectral maps were composed of 65 (43) consecutive spectra recorded at excitation energies ranging from 2818 to 2831 eV with an energy step of 0.2 eV (0.3 eV). The acquisition time for a single spectrum was 10 s. Two consecutive RIXS (10–16 REXS) series were recorded in order to collect more statistics and also to check the general reproducibility of the measurement. To check for the photo-chemical stability of the target fast (~30 s duration time) TFY scans were performed before and after every RIXS and REXS series of measurements. The spectra were then corrected for the target self-absorption. In order to accurately model the RIXS cross section the knowledge of the experimental spectral resolution is essential. A typical value of 0.63 eV was obtained from a fitting procedure on the elastic peak.

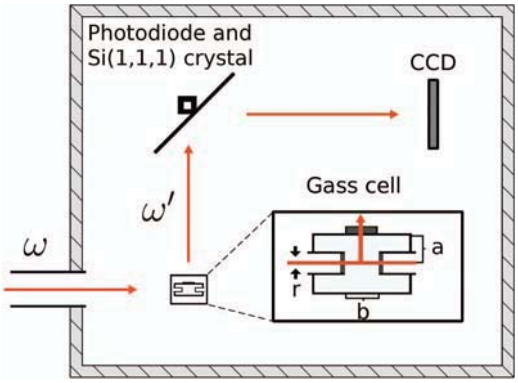

FIG. 1. Experimental scheme of the JSI high resolution x-ray spectrometer installed on ID26 beamline of ESRF. The red arrows indicate the direction of incoming and outgoing photons. The later are scattered on the Si(111) crystal and detected by the CCD camera. The parameters r, a, and b are important to model the self-absorption correction (Appendix A).

III. THEORY

A. Electronic configuration

The molecular symmetry of chloromethanes varies with the number of chlorine and hydrogen atoms. While CH_2Cl_2

TABLE I. Ground state electronic configuration for CH_3Cl, CH_2Cl_2, $CHCl_3$, and CCl_4 as calculated by StoBe deMon.[30]

Molecule	Cl 1s	C 1s	Cl 2s	Cl 2p
CH_3Cl	$1a_1^2$	$2a_1^2$	$3a_1^2$	$3a_1^2\ 1e^4$
CH_2Cl_2	$1b_1^2 1a_1^2$	$2a_1^2$	$2b_1^2 3a_1^2$	$4a_1^2 3b_1^2 5a_1^2 4b_1^2 1a_2^2 1b_2^2$
$CHCl_3$	$1e^4 1a_1^2$	$2a_1^2$	$2e^4 3a_1^2$	$4a_1^2 3e^4 4e^4 1a_2^2 5a_1^2 5e^4$
CCl_4	$1t_2^6 1a_1^2$	$2a_1^2$	$2t_2^6 3a_1^2$	$4a_1^2 3t_2^6 1e^4 4t_2^6 1t_1^6$
Molecule		Occupied valence orbitals		Unoccupied valence orbitals
CH_3Cl		$5a_1^2 6a_1^2 2e_1^4 7a_1^2 3e_1^4$		$\underbrace{8a_1^0}_{1\text{st }\sigma^*}$
CH_2Cl_2		$6a_1^2 5b_1^2 7a_1^2 2b_2^2 8a_1^2 6b_1^2 9a_1^2 2a_2^2 7b_1^2 3b_2^2$		$\underbrace{10a_1^0}_{1\text{st }\sigma^*}\ \underbrace{8b_1^0}_{2\text{nd }\sigma^*}$
$CHCl_3$		$6a_1^2 6e^4 7a_1^2 8a_1^2 7e^4 8e^4 9e^4 9a_1^2 2a_2^2$		$\underbrace{10a_1^0}_{1\text{st }\sigma^*}\ \underbrace{8e^0}_{2\text{nd }\sigma^*}$
CCl_4		$5a_1^2 5t_2^6 6a_1^2 6t_2^6 2e^4 7t_2^6 2t_1^6$		$\underbrace{7a_1^0}_{1\text{st }\sigma^*}\ \underbrace{8t_2^0}_{2\text{nd }\sigma^*}$

possesses the lowest symmetry, C_{2v}, CH_3Cl, and $CHCl_3$ are of higher C_{3v} symmetry, and CCl_4 is the most symmetrical with T_d symmetry. The electronic ground state configurations obtained by a density functional theory (DFT) optimization of the ground electronic state are given in Table I.

The core orbitals of all molecules consist of atomic like carbon 1s and chlorine 1s, 2s, and 2p orbitals, while chlorine 3s and 3p, carbon 2s and 2p, and hydrogen 1s orbitals compose unoccupied and occupied valence molecular orbitals. The LUMO, labeled as the 1st σ^* orbital, is an antibonding orbital with a nodal plane between the chlorine 3$p\sigma$ and carbon 2s/2$p\sigma$ orbitals. While there is only one chlorine 3$p\sigma$ orbital available in CH_3Cl, there are 2, 3, and 4 chlorine 3$p\sigma$ orbitals, respectively, in the other molecules, which, when making linear combinations, form a second type of σ^* orbitals (see in Figure 2). Since these 2nd σ^* orbitals in $CHCl_3$ or CCl_4 transform as the same irreducible representation, they are degenerate.

B. Computational method

Over the years the processes of core-excitations and core ionizations have been more or less accurately modeled by a wide variety of methods.[31–35] The transition potential (TP) approach[36] is a DFT method where an electronic state is optimized with half of an electron missing in the core orbital of interest. It follows that in this approximation the excitation energies can simply be expressed as differences in orbital energies between the core orbital and virtual orbitals, while the oscillator strengths are proportional to the squares of the corresponding electric dipole moments, due to orthogonality of the TP orbitals. In contrast to the transition state method first introduced by Slater,[37] the similar TP approach allows one to obtain the whole x-ray absorption near-edge spectrum by optimizing a single state. While this method accurately estimates excitation energies of bound states, it does so also for unbound states, with the only difference being the negative virtual orbital energies. As the energy of unbound states becomes higher, more diffuse functions are needed for their description. A computationally efficient double basis set technique,[35,36] where after the convergence of the half-occupied core hole state an augmentation basis set is appended to the original one in a final diagonalization, has proven to be very effective in describing Rydberg and unbound states. In that manner, oscillator strengths of the continuum can be simulated up to approximately 10 eV above the absorption edge.

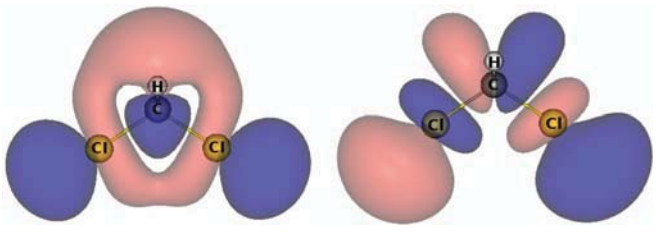

FIG. 2. The 1st (left) and 2nd (right) σ^* orbitals obtained in the ground state optimization of CH_2Cl_2. The red and blue colors represent the negative and positive values of the wave function, respectively.

In order to obtain a more accurate absolute energy scale and relative excitation energies the TP approach is often combinated with the Delta-Kohn-Sham method (ΔKS),[36] in which the relaxation effects of core-excited states are accurately taken into account. In the first step, the optimization of the lowest core-excited state with an electron in the LUMO is made. In further steps, the optimization of the nth lowest core excited state is made by removing LUMO, LUMO+1, ..., and LUMO+(n − 1) from the variational space forcing the core electron to occupy LUMO+n. With this procedure, it is possible to accurately calculate only the energies of a few low-lying well-separated resonances, because it breaks down when the density of states becomes too high or when the character of the state becomes too diffuse.

IV. RESULTS AND DISCUSSION

A. Absorption

All x-ray absorption calculations were performed using the DFT based program package StoBe.[30,36] After geometry optimization, two sets of TP calculations were performed, one employing the full symmetry of the molecule and the other without the symmetry constraint resulting in a fully localized 1*s* core hole on one of the chlorine atoms. For all TP calculations the exchange functional of Becke[38] was employed together with the gradientless correlation functional based on pair-correlation function.[39] The IGLO-III basis set,[40] known to properly describe core relaxation effects, for chlorine and cc-pVTZ and (3111/111) basis sets for carbon and hydrogen atoms were taken for the primary basis, while a large (19*s*,19*p*,19*d*) set of highly diffuse functions was used for the augmentation basis. The results of the TP calculations are gathered in Table II.

Apart from the different absolute energy scale obtained in calculations with and without symmetry constraints, a noticeable difference in the oscillator strengths ratio for the 1st and 2nd σ^* resonances is observed. While in calculations without the symmetry constraint this ratio is approximately 0.3 for all molecules with more than one chlorine atom, it is around 1 or even more in calculation employing the full symmetry. In addition, the energy difference between the two σ^* resonances is somewhat larger in the no-symmetry calculations. For CH_3Cl, no noticeable difference between the two calculations can be observed, since the core orbital is already well localized in the calculation employing symmetry.

In order to improve the absolute energy scale of the calculated spectra and the relative energies of some low-lying valence and Rydberg states of the TP calculation without the symmetry constraint, the ΔKS method was performed. A flexible augmented correlation consistent polarized valence quadruple zeta basis set (aug-ccPVQZ)[41] with two additional diffuse *s*, *p*, and *d* functions on chlorine atoms was used in order to properly describe states with an electron in a diffuse orbital, while again cc-pVTZ and (3111/111) basis sets were used for carbon and hydrogen atoms. The PD86[42] and PBE[43] were taken for the exchange and correlation functionals. For CH_2Cl_2, $CHCl_3$, and CCl_4 the 1st σ^*, 2nd σ^*, and 4*s* resonances were ΔKS corrected, while for CH_3Cl the ΔKS method was applied on 1st σ^*, 4*s*, and 4*p* resonances.

For a comparison with the experimental data a broadening of the calculated spectrum was performed. All resonances below the ionization potential (IP) were broadened by a Lorentzian function of 0.64 eV FWHM describing the natural lifetime of the 1s hole in Cl,[44] while resonances above the threshold were broadened by a Gaussian function. Because above-IP states become more sparse and intense with increasing energy, an artificial linear increase of the broadening was performed in order to smooth out the continuum contribution. In that manner the broadening was increased linearly from 0.64 eV to 6.4 eV at photon energy 10 eV above the ionization threshold. Finally, the calculated absorption spectra were convoluted with a Gaussian function of 0.4 eV corresponding to the energy resolution of the incoming photon beam. An energy shift of approximately 2 eV, mainly due to relativistic effects and functional dependence[45] was applied in the end in order to match the energy position and intensity of the 1st σ^* resonance in the experimental spectra (Figure 3).

The calculated spectra are in fair agreement with the experimental ones. Peaks A, B, and C are assigned to promotions of chlorine 1*s* electrons to the 1st σ^*, 2nd σ^*, and 4*p* orbitals. Structure D, lying above the edge, is most likely a shape resonance due to the molecular field caused by highly electronegative chlorine atoms, but could also include two-electron transitions as shake-up and shake-off processes.[2,46] Our simulations with FEFF code[47] indicate that weak undulation of the photoabsorption cross section at about 2835 eV can be ascribed to the onset of the EXAFS signal which extends

TABLE II. Excitation energies (in eV) and normalized oscillator strengths of low-lying resonances calculated with the TP method with ([1]) and without ([2]) symmetry constraints.

CH_3Cl					CH_2Cl_2				
Resonance	Exc. en.[1]	Exc. en.[2]	Osc.[1]	Osc.[2]	Resonance	Exc. en.[1]	Exc. en.[2]	Osc.[1]	Osc.[2]
$8a_1$/1st σ^*	2814.60	2814.78	1.000	1.000	$10a_1$/1stσ^*	2814.36	2777.88	1.000	1.000
/	/	/	/	/	$8b_1$/2ndσ^*	2816.03	2778.95	0.215	0.756
4*s*	2816.60	2816.89	0.003	0.003	4*s*	2816.85	2780.25	0.003	0.012
4*pπ*	2817.72	2818.12	0.017	0.017	$4p_1$	2817.68	2781.16	0.008	0.005
4*pπ*	2817.72	2818.12	0.017	0.017	$4p_2$	2818.04	2781.62	0.083	0.062
4*pσ*	2817.92	2818.34	0.098	0.090	$4p_3$	22818.20	2781.69	0.060	0.011
$CHCl_3$					$CHCl_4$				
Resonance	Exc. en.[1]	Exc. en.[2]	Osc.[1]	Osc.[2]	Resonance	Exc. en.[1]	Exc. en.[2]	Osc.[1]	Osc.[2]
$10a_1$/1st σ^*	2814.08	2775.97	1.000	1.000	$7a_1$/1st σ^*	2813.76	2757.91	1.000	1.000
10*e*/2nd σ^*	2815.70	2777.32	0.237	0.420	$8t_2$/2nd σ^*	2815.35	2759.32	0.254	0.620
10*e*/2nd σ^*	2815.97	2777.32	0.053	0.432	$8t_2$/2nd σ^*	2815.66	2759.32	0.044	0.327
/	/	/	/	/	$8t_2$/2nd σ^*	2815.66	2759.32	0.044	0.913
4*s*	2817.11	2778.74	0.001	0.003	4*s*	2817.67	2761.59	0.016	0.006
$4p_1$	2818.05	2779.74	0.053	0.026	$4p_1$	2818.46	2762.40	0.067	0.062
$4p_2$	2818.38	2780.01	0.065	0.061	$4p_2$	2818.55	2762.40	0.037	0.064
$4p_3$	2818.40	2780.01	0.047	0.058	$4p_3$	2818.56	2762.40	0.032	0.066

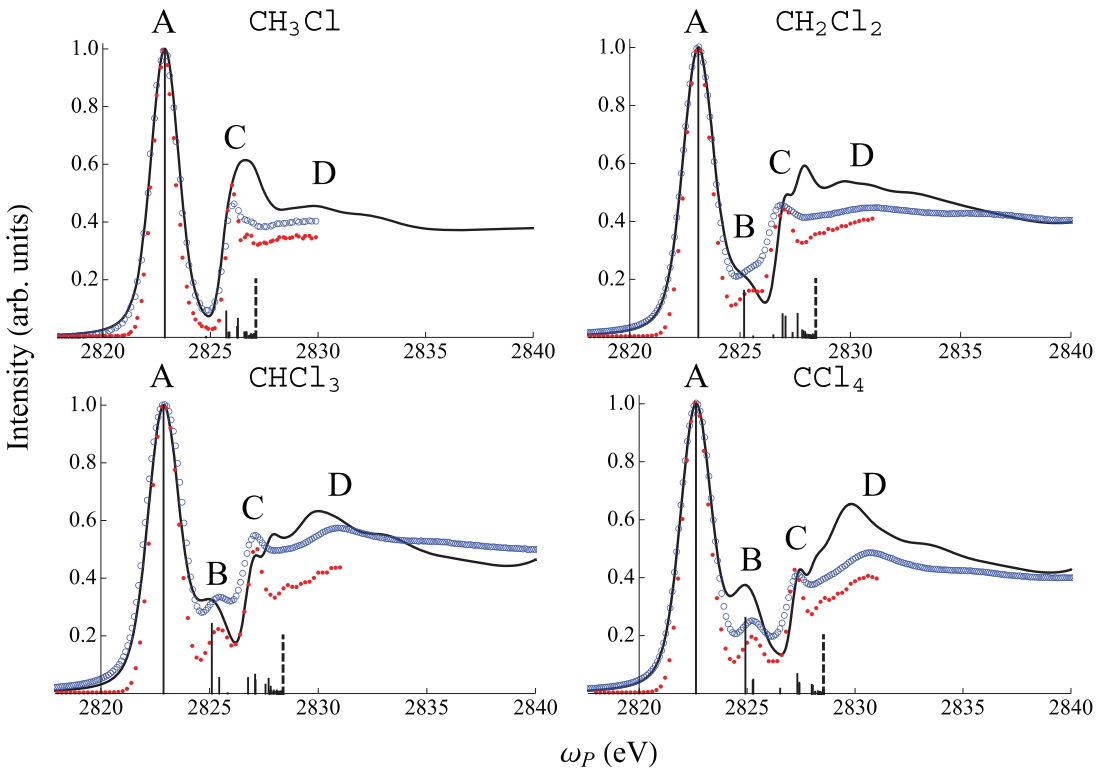

FIG. 3. A comparison of measured total fluorescence yield spectra at Cl K-edge (blue circles) with calculated absorption spectra not employing the symmetry constraint (black curve). In addition, measured HERFD (see text) spectra taken at the resonant emission energy are appended (red dots). The oscillator strengths for states below the ionization edge (dashed vertical line) are indicated by vertical solid lines. In order to obtain a better agreement with the measurements, expression (C4) of Appendix C was used to describe the first two resonances with FC widths given in Table IV.

towards higher photon energies. The energy positions of calculated and measured peaks along with their assignments are given in Table III. We observe that peak B is missing in the spectrum of CH_3Cl. This is due to the fact, that the molecule with one chlorine atom does not form the 2nd σ^* resonance. The comparison of the two sets of TP calculations with the experimental data by A versus B relative peak intensity (approximately 0.3) and their energy difference (larger than 2 eV) indicates a localization of the core hole and a symmetry breaking (see Table II). As a consequence, the degeneracy of 2nd σ^* orbitals is lifted and although this effect cannot be resolved in our absorption spectra, it has been observed in electron energy loss spectra of the related $CFCl_3$ molecule.[10] In all our TP calculations, the intensity of resonances above the 4*p* resonance is overestimated, resulting in an artificial peak located around the IP which is not resolved in the experimental spectra. We found a functional dependence on the intensity of this peak and chose a combination of exchange and correlation functionals giving the lowest intensity.

Figure 3 also contains counts from horizontal slices of RIXS spectral maps recorded at the resonance emission energy. Peaks from these so called High Energy Resolution Fluorescence Detected (HERFD) x-ray absorption spectra[48,49] are unaffected by the lifetime broadening of the intermediate state and are thus narrower than the corresponding peaks recorded in the TFY mode. From the HERFD spectra it can clearly be seen that the first two resonances are much broader compared to the 4*p* peak, indicating a dissociative character of the former. This is quite clear by looking at the corresponding orbital picture (see Figure 2). Namely, both orbitals are composed of chlorine 3*p* and carbon 2*s*/2*pσ* orbitals with two nodal planes in between the two atoms, but appear in different

TABLE III. Assignment and experimental and theoretical energy positions of A–D marked in Figure 3 (all units are in eV). The theoretically determined (no-symmetry TP and ΔKS) energy positions of peaks B and C were taken as the weighted average of the corresponding resonance energies, since our calculations indicate a small energy splitting.

	CH_3Cl			CH_2Cl_2			$CHCl_3$			CCl_4		
Peaks	Ass.	Expt.	Theory	Ass.	Expt.	Theory	Ass.	Expt.	Theory	Ass.	Expt.	Theory
A	1st σ^*	2822.85	2820.97	1st σ^*	2823.11	2820.77	1st σ^*	2822.89	2820.59	1st σ^*	2822.66	2820.26
B	/	/	/	2nd σ^*	2825.51	2822.85	2nd σ^*	2825.44	2822.87	2nd σ^*	2825.33	2822.65
C	4*p*	2825.97	2823.86	4*p*	2826.85	2824.50	4*p*	2827.12	2824.70	4*p*	2827.24	2825.01
IP		/	2825.20		/	2826.10		/	2826.09		/	2826.17
D	Shape	/	2827.89	Shape	2830.91	2827.42	Shape	2830.95	2827.70	Shape	2830.81	2827.46

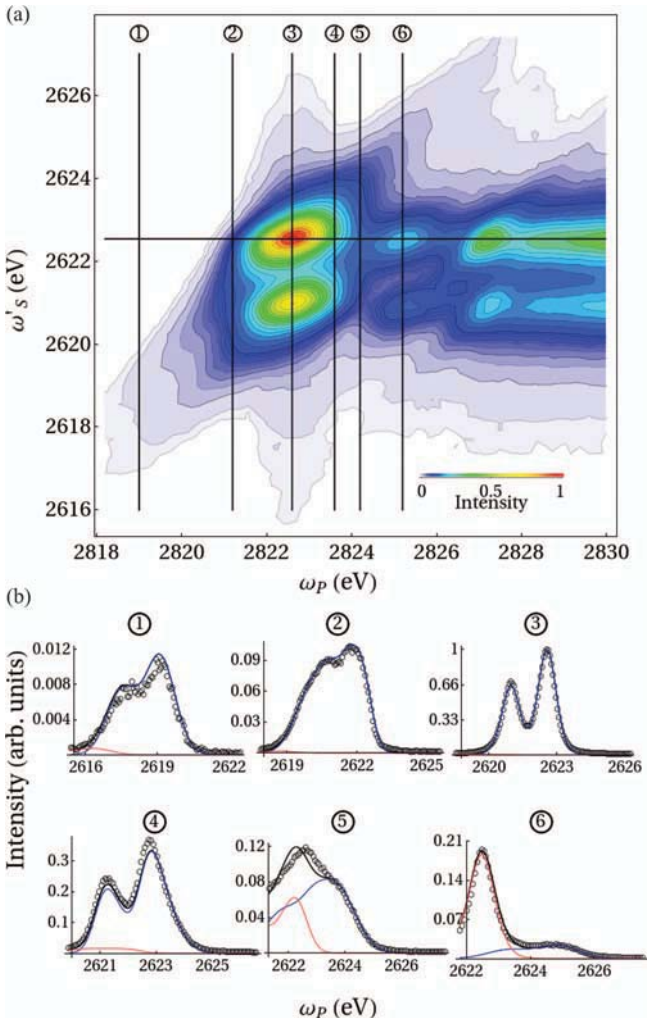

FIG. 4. (a) Experimental K_α RIXS map for CCl4 with the horizontal line marking the HERFD absorption spectra as reported in Figure 3. (b) A comparison between the experimental (black dots) and fitted (black line) emission spectra from CCl_4, recorded at various energy detunings relative to the 1st and 2nd resonances. The blue and red lines indicate the contribution of the 1st and 2nd σ^* resonances to the total yield.

linear combinations. Nevertheless, the repulsive force is comparable in both cases resulting in a considerable FC width.

B. RIXS

In order to extract the FC widths from the experimental RIXS maps, a model function employing corrections due to experimental broadening was employed to fit the experimental data, as described in Appendix C (Eq. (C7)). Two functions centered at the resonant excitation energies of the two σ^* resonances were pinpointed so that their intensities match the intensity of the two experimental peaks at their maximum. Only (ω_P, ω'_S) points with negligible contributions from $4s$ and $4p$ resonances were used in the fitting procedure, i.e., $K\alpha_{1,2}$ points of the 1st σ^* resonance and $K\alpha_1$ points of the 2nd σ^* resonance for photon impact energy up to the resonance energy of the 2nd σ^* resonance. The FC widths of the 1st and 2nd resonances along with the final state spin-orbit splittings and spin-orbit rates were taken as parameters, while the lifetime broadening and the total experimental resolution was kept constant. Molecular field effects,[27,50] which split the final state into two components, were not taken into account, but since this splitting is small (approximately 0.3 eV), we estimate that these contributions have a minor effect. A generally good fit was obtained for all the molecules in this study. In Figure 4, we show experimental RIXS maps along with some vertical slices with fits made at several impact photon energies for CCl_4. Discrepancies at incoming photon energies lying between the energies of the two σ^* resonances may be due to the interference effects[25] which are neglected in our model.

As seen in Figure 5, the model functions of the 1st and 2nd σ^* resonances accurately fit the positions of the peak maxima and the widths of the emission spectra recorded at different excitation energies. For this, the model contribution of the second resonance obtained by the above mentioned fit was subtracted from the experimental data to get a clear signal of the first resonance, and vice versa. Such "isolated" resonance spectra were then fitted individually in order to determine the positions of the emission maxima and the widths. As

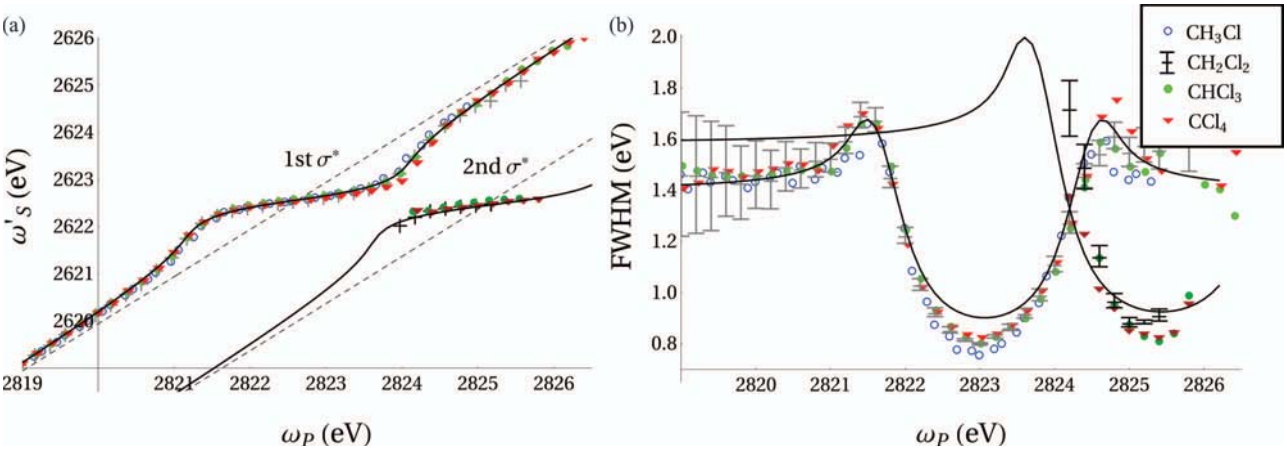

FIG. 5. (a) Measured dispersion curves and (b) widths of K_α emission lines as a function of incoming photon energy for the 1st (lighter symbols) and 2nd (darker symbols) σ^* resonances together with the dispersions and the widths for CH_2Cl_2 generated by the fit (black lines). The experimental error bars for CH_2Cl_2 in (b) are representative for all four studied molecules.

TABLE IV. The FC widths of the 1st and 2nd σ^* resonances determined from the fit.

	CH_3Cl (eV)	CH_2Cl_2 (eV)	$CHCl_3$ (eV)	CCl_4 (eV)
$\Delta_{1st\,\sigma^*}$	1.133 ± 0.041	1.254 ± 0.042	1.311 ± 0.041	1.301 ± 0.035
$\Delta_{2nd\,\sigma^*}$	/	1.45 ± 0.37	1.51 ± 0.27	1.41 ± 0.26

expected, the linear coefficients describing the slopes of the dispersions at the resonant excitation energies for the two σ^* resonances are smaller than one (Figure 5(a)) and the widths of the emission peaks decrease as the incoming photon energy approaches the resonant energy (Figure 5(b)). The discrepancy of the widths on top of the resonance is most probably due to an overestimation of the experimental resolution. What is surprising is that the dispersion curve and the width curve are very similar for all four molecules. Since the FC width depends on the mass ratio of the molecular fragments[23] which varies strongly across the chloromethane series, larger differences were expected. In an earlier RIXS study involving the Cl K shell excitations to the 1st σ^* resonance of CF_3Cl, CF_2Cl_2, $CFCl_3$, and CCl_4[11] the same observation was made. This indicates that the dissociation rate of the chloro-fluoromethanes primarily depends on the two atoms connected with a σ^* bond (C–Cl) and not significantly on the mass of other atoms in the molecule. A detailed theoretical analysis of the ground and excited potential energy surfaces (PES) would be necessary in order to confirm this observation.

The resulting FC widths from the fits with a fixed experimental resolution (Table V) and lifetime broadening (0.64 eV) are given in Table IV. The FC widths of the 1st resonance for CH_2Cl_2, $CHCl_3$, and CCl_4 are all the same within the estimated error, while, compared to the other three molecules, a slightly poorer fit for CH_3Cl gives approximately a 0.2 eV lower FC width. This value did not change substantially even if the constraint of a fixed lifetime broadening and the experimental resolution was lifted. In an earlier CH_3Cl study a FC width of 1.3 eV was obtained from the fit, but the experimental resolution was not taken into account.[28] However, as indicated by our calculation, the effect of applying an experimental broadening is essential, as this increases the magnitude of the resonance tails with respect to its maximum. If the experimental broadening is not taken into account, another parameter has to change in order for the tail region to increase. The compensation is done most easily by increasing the lifetime broadening, but this would automatically change the FC width because the two quantities are strongly correlated in the fit.

The FC widths of the 2nd σ^* resonances seem to have systematically higher values compared to those of the first resonance but also a much larger uncertainty due to a relatively smaller intensity and the influence of the near lying 4*s* and 4*p* resonances. In addition, our calculations indicate that there may be a splitting of approximately 0.3 eV in this resonance for $CHCl_3$ and CCl_4 due to the symmetry breaking. Since the experimental sampling of the excitation energy is too low to clearly observe that effect, a single function was used to fit the 2nd σ^* resonance. The obtained values of the FC widths for the second resonance are therefore rather qualitative, but most importantly, they are different from zero indicating a dissociation process triggered by core excitation to the 2nd σ^* orbital.

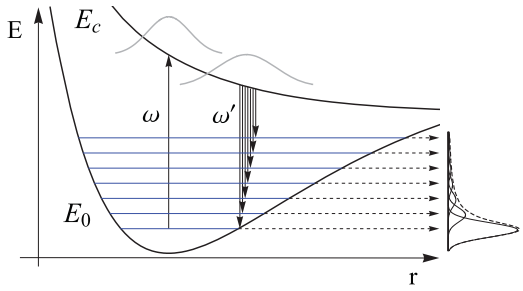

FIG. 6. A scheme of the resonant elastic scattering involving PES of the ground state (E_0) and the dissociative core-excited (E_c) state. Upon resonant excitation from the ground vibrational state the molecule may de-excite into higher vibrational levels of the ground electronic state (blue lines). The contributions from individual vibrational excited states to the emission spectra (solid curves) as well as their overall contribution (dashed curve) are shown along the vertical axis.

C. REXS

As already noted by Simon *et al.*,[22] the peaks corresponding to elastically scattered photons to dissociative resonances assume an asymmetric shape when the energy of the incoming photons approaches the resonant energy. Since the effective scattering time[24] is larger at zero energy detuning of the resonance, the atoms have more time to evolve from the equilibrium positions and when de-excitation to the ground state takes place, the transition probability for excitation to higher vibrational states becomes higher. Because the de-excitation energy to higher vibrational states is smaller compared to the de-excitation energy to the ground vibrational state, these emission peaks appear on the lower energy side of the primary peak and cause its asymmetry (Figure 6).

In our experimental setup the direction of the outgoing photon beam is along the polarization axis of the incoming photon beam, so that the measured elastic scattering signal is solely due to the resonant scattering. Since this signal lies in the tail region of the more intense K_β emission line (Figure 7(a)), a linear background was subtracted from the experimental spectra to separate the signal of elastically scattered photons. In order to highlight the asymmetry of emission peaks in our experimental data, a fit with a Gaussian function at four different photon probe energies was performed: 3 eV below the 1st σ^* resonance, top of the 1st σ^* resonance, top of the 2nd σ^* resonance, and top of the 4*p* Rydberg resonance (Figure 7(b)). For REXS spectra taken on top of the non-dissociative 4*p* resonance and for those recorded in the tail region of the 1st σ^* resonance, with a reduced effective scattering time, no significant deviation from the symmetric shape is observed. On the other hand, the emission spectra recorded at the top of the 1st and 2nd σ^* resonances exhibit asymmetry, as seen in Figures 7(c) and 7(d) for all four molecules. As the asymmetry is clearly visible on top of the 1st σ^* resonance, the effect is not so pronounced in the case of the 2nd σ^* resonance. This is due to a relatively smaller share of the 2nd σ^* resonance signal in comparison with the signal tail from the 1st σ^* resonance at the top of the

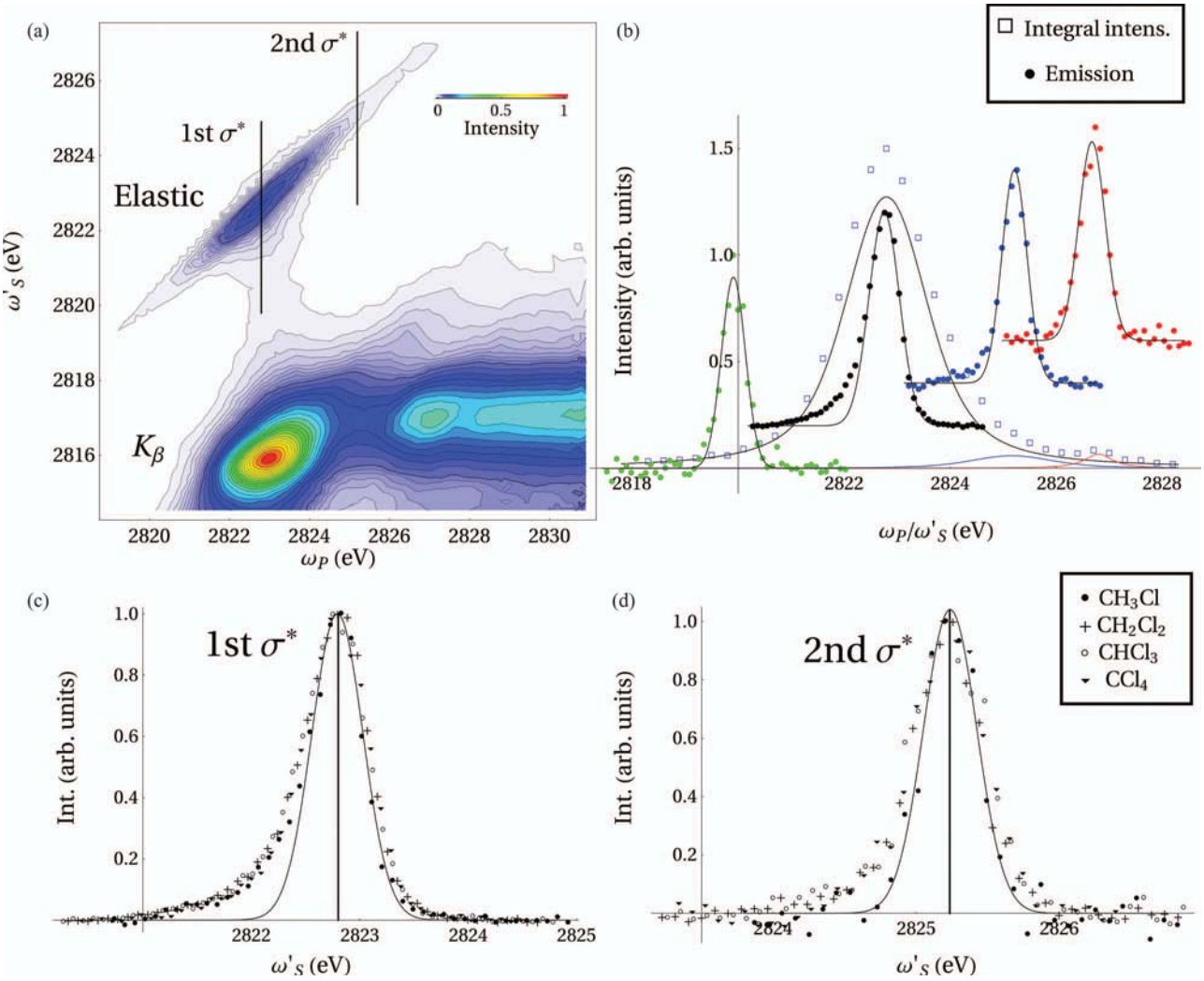

FIG. 7. (a) Experimental RIXS map in the region of elastic and K_β emission line for CH_2Cl_2. (b) Emission spectra of elastically scattered photons of CH_2Cl_2 recorded at different absorption energies along with their integral intensity. The solid black, blue, and red lines represent the modeled integral intensity contributions from the 1st σ^*, 2nd σ^*, and 4p resonances, respectively. (c) and (d) show emission spectra recorded at zero detuning from the 1st and 2nd σ^* resonances for all four molecules.

2nd σ^* resonance excitation. Namely, the cross section ratio is proportional to the 4th power of the dipole matrix element ratio as compared to the absorption with a quadratic dependence on the matrix element ratio. At this incoming photon energy the effective scattering time of the 1st σ^* resonance is too short (corresponding to 2.3 eV energy detuning) to enable the molecule to rearrange and significantly excite higher vibrational modes as the de-excitation to the electronic ground state takes place. The emission signal is thus composed of a fairly symmetric signal from the 1st σ^* resonance and the contribution from the 2nd σ^* resonance, which gives an overall peak asymmetry. The effect of the 2nd σ^* resonance on the overall peak asymmetry can be clearly observed if we compare the emission spectra of CH_3Cl and CH_2Cl_2, $CHCl_3$, and CCl_4 recorded at the resonant energy of the 2nd σ^* resonance. Since CH_3Cl does not form the 2nd σ^* resonance, the elastic scattering spectrum is symmetric in contrast to the other three molecules (Figure 7(d)).

Finally, we have extracted the total elastic yield as a function of the photon probe energy by integrating the measured elastic scattering signal over the emitted photon energy (Figure 7(b)). The integrated elastic yield was modeled by employing Eq. (C6) of Appendix C, with relative intensities of the resonant peaks scaled according to the calculated oscillator strengths from Table II, and the FC widths taken from Table IV. Since Eq. (C6) applies only for transition to the ground vibrational state, we have estimated the contribution of the higher vibrational modes by taking the ratio between the surface area under the Gaussian function and its residuum in the emission spectra recorded at the top of the 1st σ^* resonance (Figure 7(c)). Consequentially, the contribution of the model signal corresponding to transitions back to the ground state was scaled to represent 0.85 share of the integrated experimental intensity.

V. CONCLUSIONS

The dissociation dynamics of chlorinated methane derivates after the Cl 1s core excitation to the 1st and 2nd σ^* resonances was experimentally and theoretically investigated

by the TFY, K_α RIXS, and REXS spectroscopies. As confirmed by our DFT calculations the virtual orbitals associated with the two lowest resonances both have a σ^*(C–Cl) character and core-excitations to such orbitals result in dissociation of the molecule. The effect of this fast nuclear dynamics was evidenced by a spectral broadening of the two σ^* resonances in the TFY and HERFD spectra, by an asymmetric broadening of peaks corresponding to the resonant elastic x-ray scattering, and as a breakdown of linear Raman dispersion accompanied by a narrowing of the emission peaks in the RIXS spectra. The FC widths for both resonances were extracted by a fitting procedure of K_α spectral maps taking into account the experimental broadening. The resulting FC widths for the 1st σ^* resonance, together with similar results obtained for the chloro-fluoro-methanes,[11] indicate that the initial dissociation dynamics for these molecules is primarily determined by the C–Cl bond with practically negligible effect of the other atoms in the molecule. Similar conclusion apply for the 2nd σ^* resonance with FC widths similar to those of the 1st σ^* resonance indicating a dissociative character of this state. The situation may be more complicated for larger molecules, such as halogenated ethanes, where the fast movement of the $(CH_2)_2$ moiety triggered by the resonant photoabsorption plays a major role in the initial dissociation dynamics.[21]

ACKNOWLEDGMENTS

We acknowledge S. Urquhart for his support on the theoretical calculations and K. Kvashnina for her assistance in tuning the ID26 beamline. This work is supported by the Slovenian Research Program P1-0112. The financial supports of the Oulu University, the Swiss National Science Foundation, and the NSERC (Canada) are also acknowledged. W.C. was funded by NSERC (Canada) when at the University of Saskatchewan.

APPENDIX A: EXTENDED EXPERIMENTAL DETAILS

The measured emitted x-ray intensity is modified by a factor of $(1 - \exp[-\mu(\omega)b])$, where μ is the frequency dependent absorption coefficient and $b = 4$ mm the target interaction length along the beam direction (see Figure 1). The proportionality factor is a product of the partial fluorescence cross section and the spectrometer efficiency. At low target pressure ($\mu b \ll 1$), the measured total fluorescence yield is directly proportional to the absorption coefficient and thus to the corresponding fluorescence cross section. If μb is large, the measured spectra have to be weighted by a factor of $\mu(\omega)b/(1-\exp[-\mu(\omega)b])$ in order to extract an experimental quantity proportional to the photoabsorption cross section.[51] Although all molecules have been measured at approximately the same vapor pressure, the density of chlorine varies substantially from molecule to molecule and μb differs considerably from zero for molecules with a high number of chlorine atoms (for CCl_4 the maximum of $\mu b \sim 0.45$). In addition, the measured REXS spectra were distorted due to self-absorption of the emitted photons. Since the photon beam diameter ($r = 0.25$ mm) is much smaller than the path length of the scattered light before the exit window ($a \approx 4$ mm), the correction due to self-absorption was approximated by the factor $\exp[\mu(\omega')a]$.

TABLE V. The total experimental energy resolution obtained by a fitting procedure of spectral lines involving elastically scattered photons on the 1st σ^* resonance and on the 4p Rydberg resonance, and their combined values δ_T.

	CH_3Cl (eV)	CH_2Cl_2 (eV)	$CHCl_3$ (eV)	CCl_4 (eV)
1st σ^*	0.62 eV ± 0.15	0.62 ± 0.09	0.65 ± 0.10	0.65 ± 0.12
4p	0.54 eV ± 0.27	0.63 ± 0.13	0.67 ± 0.16	0.70 ± 0.20
δ_T	0.60 ± 0.13	0.62 ± 0.07	0.65 ± 0.09	0.66 ± 0.10

APPENDIX B: EXPERIMENTAL RESOLUTION

Since the broadening of emission lines resulting from elastically scattered photons depends only on the combined energy resolution of the spectrometer and the incoming photon distribution, the total experimental resolution can in principle be easily extracted by fitting the elastic emission spectrum by a model function. Spectra recorded at two incoming photon energy regions are considered. The first region corresponds to large negative detunings with respect to the 1st σ^* resonance. The effective scattering time in this region is long so that contributions from vibrational excitations are low. The second region corresponds to incoming photon energies near the non-dissociative 4p resonance. The signal in this region is weak but is free from asymmetrical broadening due to fast dissociation. The corresponding spectra were fitted by a combination of a Gaussian and a linear function in order to take the offset from low-energy lying intense inelastic emission peaks into account (see Figure 7(a)). The obtained values for the total experimental resolution δ_T along with the estimated errors are reported in Table V.

APPENDIX C: CROSS SECTIONS

The contribution from the ith excited electronic state to the photoabsorption cross sections and of the fth final electronic state to the cross section for resonant x-ray scattering (RXS)[23] have the following form (in atomic units) in the Born-Oppenheimer approximation:

$$\sigma^i_{abs}(\omega) = 4\pi^2\alpha\omega \sum_c \int |H^i_c|^2 \frac{\Gamma/2\pi}{\left(\omega - \omega^i_{c0}\right)^2 + \Gamma^2/4} dE^i_c, \qquad H^i_c = D_{i0}\langle\phi^i_c|\phi_0\rangle, \tag{C1}$$

$$\sigma^{fi}_{RXS}(\omega,\omega') = \alpha^4\frac{\omega'}{\omega}\sum_{c'}\int |F^{fi}_{c'}|^2\delta(\omega' - \omega + \omega^f_{c'0})dE^f_{c'}, \qquad F^{fi}_{c'} = \sum_c \int D_{fi}D_{i0}\frac{\langle\phi^f_{c'}|\phi^i_c\rangle\langle\phi^i_c|\phi_0\rangle}{\omega - \omega^i_{c0} + i\Gamma/2}dE^i_c, \tag{C2}$$

where ω and ω' are the frequencies of incoming and outgoing photons, D_{fi} and D_{i0} are the electronic dipole moments between the final and intermediate and intermediate and ground

state, respectively, Γ is the lifetime broadening of the intermediate core-hole states and $|\phi_c^i\rangle$ and $|\phi_{c'}^f\rangle$ are the intermediate and final state nuclear wave functions whose energies are E_c^i and $E_{c'}^f$, respectively. The energy differences between the nuclear wave function of the ground vibronic state $|\phi_0\rangle$ with energy E_0 and the intermediate and final states are labeled ω_{c0}^i and $\omega_{c'0}^f$. In both equations, we have left the option for the intermediate and final state wave functions to either have a bound, i.e., PES with a local minimum, or a continuous, i.e., PES without a local minimum, character (the sum/integral sign). Interferences between different electronic states[25] as well as the lifetime broadening of the final state have been neglected in Eq. (C2).

The squares of the overlap integrals between nuclear wave functions are known as the Franck-Condon (FC) factors and in case of dissociative PES form a continuous distribution. For steep PES slopes of the intermediate state and for broad potential wells of the ground state PES this distribution can be estimated by a Gaussian function:[23]

$$\left|\langle\phi_c^i|\phi_0\rangle\right|^2(E_c^i) \propto \exp\left[-\frac{\left(E_c^i-\tilde{E}_c^i\right)^2}{\Delta_i^2}4\ln 2\right], \tag{C3}$$

where $\tilde{E}_c^i$ is the energy of state $|\phi_c^i\rangle$ at the equilibrium ground state geometry and Δ_i is the FWHM of the distribution and will be referred to as the FC width. Inserting Eq. (C3) into (C1) we obtain

$$\sigma_{abs}^i(\omega) \propto D_{i0}^2 \;\; V(\omega-\tilde{\omega}_{i0}, \Delta_i/2\sqrt{2\ln 2}, \Gamma/2), \tag{C4}$$

where $\tilde{\omega}_{i0} = \tilde{E}_c^i - E_0$ and $V(\Omega, \sigma, \Gamma/2)$ is the Voigt function, i.e., a convolution of a Gaussian function with the standard deviation equal to σ and a Lorentzian function with the FWHM equal to Γ. The second order cross section for dissociative resonances is in general more complicated, but assumes a simple expression if the PES of the intermediate and of the final states are parallel.[23] This is usually a valid approximation when both intermediate and final states have a deep core-hole, as in the case of KL emission. The distribution $\langle\phi_{c'}^f|\phi_c^i\rangle$ is then replaced by a delta function and the RIXS cross section can be written as

$$\sigma_{RIXS}^{fi}(\omega,\omega') \propto D_{fi}^2 D_{i0}^2 \frac{\Gamma/2}{\Omega_{fi}'^2+\Gamma^2/4} \times \exp\left[-\left(\frac{\Omega_{fi}'-\Omega_{i0}}{\Delta_i}\right)^2 4\ln 2\right], \tag{C5}$$

where $\Omega_{i0} = \omega - \tilde{\omega}_{i0}$ and $\Omega_{fi}' = \omega' - \tilde{\omega}_{fi}$ are the energy detunings of the absorbed and emitted photons with respect to the resonant absorbed and emitted central energy and $\tilde{\omega}_{fi} = \tilde{\omega}_{c0} - \tilde{\omega}_{f0}$. Another simplification occurs in the case of resonant elastic scattering, where the PES of the ground and final state are the same and $\langle\phi_{c'}^f|\phi_c^i\rangle = \langle\phi_c^i|\phi_0\rangle$, i.e., for the case of the ground vibrational state de-excitation. Equation (C2) with $\omega_{c'0}^f = 0$ then takes the following form:

$$\begin{aligned}\sigma_{REXS}^{0i}(\omega,\omega') &\propto D_{i0}^4 \left|\frac{\Delta_i}{\Gamma}\sqrt{\frac{\pi^3}{\ln 2}}\left(\Omega - i\frac{\Gamma}{2}\right)\right. \\ &\times V(\Omega, \Delta_i/2\sqrt{2\ln 2}, \Gamma/2) \\ &\left. - \int_{-E_D}^{\infty} \exp\left[-\left(\frac{\epsilon}{\Delta_i}\right)^2 4\ln 2\right]\frac{\epsilon}{(\Omega-\epsilon)^2+\Gamma^2/4}d\epsilon\right|^2 \\ &\times \delta(\omega-\omega'),\end{aligned} \tag{C6}$$

where E_D is the kinetic energy of molecular fragments when the molecule has completely dissociated.

When comparing the calculated spectra to the experimental ones, a convolution with the incoming photon distribution and, in case of RIXS and REXS, with the spectrometer response function has to be performed. An additional broadening due to the incoming photon convolution can be approximated by increasing the width of the spectrometer response function to the total experimental width. The cross section expressions used in the fitting procedures in Sec. IV are thus of the following form:

$$\begin{aligned}\hat{\sigma}_{abs}(\omega_P) &= \int \sum_i \sigma_{abs}^i(\omega)\Phi(\omega-\omega_P, \delta_P)d\omega, \\ \hat{\sigma}_{RXS}(\omega_P,\omega_S') &= \int \sum_f \sigma_{RXS}^{fi}(\omega_P,\omega')\Phi(\omega'-\omega_S', \delta_T)d\omega',\end{aligned} \tag{C7}$$

where the response function Φ is approximated by a Gaussian function and δ_T and δ_P are the total experimental energy broadening and the energy broadening of the incoming photon distribution, respectively.

[1] J. Fauvarque, Pure Appl. Chem. **68**, 1713 (1996).
[2] A. P. Hitchcock and C. E. Brion, J. Electron Spectrosc. Relat. Phenom. **14**, 417 (1978).
[3] J. L. Dehmer, J. Chem. Phys. **56**, 4496 (1972).
[4] T. D. Thomas, J. Am. Chem. Soc. **92**, 4184 (1970).
[5] E. J. Aitken, M. K. Bahl, K. B. Bomben, J. K. Gimzewski, G. S. Nolan, and T. D. Thomas, J. Am. Chem. Soc. **102**, 4873 (1980).
[6] F. P. Larkins and R. A. Phillips, J. Chem. Phys. **88**, 5323 (1988).
[7] R. C. C. Perrera, R. E. LaVilla, and G. V. Gibbs, J. Chem. Phys. **86**, 4824 (1987).
[8] M. J. Molina, Pure Appl. Chem. **68**, 1749 (1996).
[9] G. Porter, Pure Appl. Chem. **68**, 1683 (1996).
[10] W. Zhang, T. Ibuki, and C. E. Brion, Chem. Phys. **160**, 435 (1992).
[11] R. Guillemin, W. C. Stolte, L. Journel, S. Carniato, M. N. Piancastelli, D. W. Lindle, and M. Simon, Phys. Rev. A **86**, 013407 (2012).
[12] G. Fronzoni and P. Decleva, Chem. Phys. **237**, 21 (1998).
[13] D. W. Lindle, P. L. Cowan, T. Jach, R. E. LaVilla, R. D. Deslattes, and R. C. C. Perrera, Phys. Rev. A **43**, 2353 (1991).
[14] R. C. C. Perrera, P. L. Cowan, D. W. Lindle, R. E. LaVilla, T. Jach, and R. D. Deslattes, Phys. Rev. A **43**, 3609 (1991).
[15] J. Söderström, N. Mårtensson, O. Travnikova, M. Patanen, C. Miron, L. J. Sæthre, K. J. Børve, J. J. Rehr, J. J. Kas, F. D. Vila, T. D. Thomas, and S. Svensson, Phys. Rev. Lett. **108**, 193005 (2012).
[16] M. Patanen, O. Travnikova, M. G. Zahl, J. Söderström, P. Decleva, T. D. Thomas, S. Svensson, N. Mårtensson, K. J. Børve, L. J. Sæthre, and C. Miron, Phys. Rev. A **87**, 063420 (2013).
[17] P. Morin and I. Nenner, Phys. Rev. Lett. **56**, 1913 (1986).
[18] H. Aksela, S. Aksela, M. Ala-Korpela, O-P. Sairanen, M. Hotokka, G. M. Bancroft, K. H. Tan, and J. Tulkki, Phys. Rev. A **41**, 6000 (1990).
[19] P. Morin and C. Miron, J. Electron Spectrosc. Relat. Phenom. **185**, 259 (2012).

[20] C. Miron, P. Morin, D. Célion, L. Journel, and M. Simon, J. Chem. Phys. **128**, 154314 (2008).
[21] O. Travnikova, V. Kimberg, R. Flammini, X. J. Liu, M. Patanen, C. Nicolas, S. Svensson, and C. Miron, J. Phys. Chem. Lett. **4**, 2361 (2013).
[22] M. Simon, L. Journel, R. Guillemin, W. C. Stolte, I. Minkov, F. Gel'mukhanov, P. Sałek, H. Ågren, S. Carniato, R. Taieb, A. C. Hudson, and D. W. Lindle, Phys. Rev. A **73**, 020706(R) (2006).
[23] F. Gel'mukhanov and H. Ågren, Phys. Rev. A **54**, 379 (1996).
[24] F. Gel'mukhanov, P. Sałek, T. Privalov, and H. Ågren, Phys. Rev. A **59**, 380 (1999).
[25] M. Kavčič, M. Žitnik, K. Bučar, A. Mihelič, S. Carniato, L. Journel, R. Guillemin, and M. Simon, Phys. Rev. Lett. **105**, 113004 (2010).
[26] S. Carniato, L. Journel, R. Guillemin, M. N. Piancastelli, W. C. Stolte, D. W. Lindle, and M. Simon, J. Chem. Phys. **137**, 144303 (2012).
[27] S. Carniato, R. Guillemin, W. C. Stolte, L. Journel, R. Taieb, D. W. Lindle, and M. Simon, Phys. Rev. A **80**, 032513 (2009).
[28] T. Marchenko, L. Journel, T. Marin, R. Guillemin, S. Carniato, M. Žitnik, M. Kavčič, K. Bučar, A. Mihelič, J. Hoszowska, W. Cao, and M. Simon, J. Chem. Phys. **134**, 144308 (2011).
[29] M. Kavčič, M. Budnar, A. Muhleisen, F. Gasser, M. Žitnik, K. Bučar, and R. Bohinc, Rev. Sci. Instrum. **83**, 033113 (2012).
[30] K. Hermann, L. G. M. Pettersson, M. E. Casida, C. Daul, A. Goursot, A. Koester, E. Proynov, A. St-Amant, D. R. Salahub, V. Carravetta, H. Duarte, C. Friedrich, N. Godbout, J. Guan, C. Jamorski, M. Leboeuf, M. Leetmaa, M. Nyberg, S. Patchkovskii, L. Pedocchi, F. Sim, L. Triguero, and A. Vela, StoBe-deMon version 3.2, 2013.
[31] H. Jørgen, Aa. Jensen, and P. Jørgensen, J. Chem. Phys. **80**, 1204 (1984).
[32] U. Ekström, P. Norman, V. Carravetta, and H. Ågren, Phys. Rev. Lett. **97**, 143001 (2006).
[33] N. Kosugi and H. Kuroda, Chem. Phys. Lett. **74**, 490 (1980).
[34] E. Runge and E. K. U. Gross, Phys. Rev. Lett. **52**, 997 (1984).
[35] H. Ågren, V. Carravetta, O. Vahtras, and L. G. M. Pettersson, Theor. Chem. Acc. **97**, 14 (1997).
[36] M. Leetmaa, M. P. Ljungberg, A. Lyubarstev, A. Nillson, and L. G. M. Petterson, J. Electron Spectrosc. Relat. Phenom. **177**, 135 (2010).
[37] J. C. Slater and K. H. Johnson, Phys. Rev. B **5**, 844 (1972).
[38] A. D. Becke, Phys. Rev. A **38**, 3098 (1988).
[39] E. I. Proynov, A. Vela, and D. R. Salahub, Phys. Rev. A **50**, 3766 (1994).
[40] W. Kutzelnigg, U. Fleischer, and M. Schindler, *NMR-Basic Principles and Progress* (Springer, Heidelberg, 1990).
[41] D. E. Woon and T. H. Dunning, Jr., J. Chem. Phys. **98**, 1358 (1993).
[42] J. P. Perdew, Phys. Rev. B **33**, 8822 (1986).
[43] J. P. Perdew, K. Burke, and M. Ernzerhof, Phys. Rev. Lett. **77**, 3865 (1996).
[44] J. A. Campbell, At. Data Nucl. Data Tables **77**, 1 (2001).
[45] O. Takahashi and L. G. M. Pettersson, J. Chem. Phys. **121**, 10339 (2004).
[46] A. F. Largo, J. Z. Davalous, U. Kerdpin, and A. S. Schlachter, J. Phys. Chem. A **110**, 13717 (2006).
[47] J. J. Rehr, J. J. Kas, F. D. Vila, M. P. Prange, and K. Jorissen, Phys. Chem. Chem. Phys. **12**, 5503 (2010).
[48] K. Hamalinen, D. P. Siddons, J. B. Hastings, and L. E. Berman, Phys. Rev. Lett. **67**, 2850 (1991).
[49] P. Glatzel, T. Weng, K. Kvashnin, J. Swarbrick, M. Sikora, E. Gallo, N. Smolentsev, and R. A. Mori, J. Electron Spectrosc. Relat. Phenom. **188**, 17 (2013).
[50] L. El Khoury, L. Journel, R. Guillemin, S. Carniato, W. C. Stolte, T. Marin, D. W. Lindle, and M. Simon, J. Chem. Phys. **136**, 024319 (2012).
[51] W. Cao, J.-Cl. Dousse, J. Hoszowska, M. Žitnik, M. Kavčič, and K. Bučar, Phys. Rev. A **81**, 012501 (2010).